High-Resolution Analysis of the S_1–S_0 Transition of Magnesium Phthalocyanine: Rotational Structure and Electronic Angular Momentum

Yuki Miyamoto[1, a)], Katsunari Enomoto[2], Kana Iwakuni[3], Susumu Kuma[4], Koichi M. T. Yamada[3]

[1]Research Institute for Interdisciplinary Science, Okayama University, Kita-ku, Okayama 700-8530, Japan

[2]Department of Physics, University of Toyama, Toyama 930-8555, Japan

[3]Institute for Laser Science, University of Electro-Communications, Chofu, Tokyo 182-8585, Japan

[4]Department of Physics, Rikkyo University, Tokyo 171-8501, Japan

a) Author to whom correspondence should be addressed.

Electronic mail: miyamo-y@okayama-u.ac.jp

We report a high-resolution spectroscopic analysis of the S_1–S_0 transition of magnesium phthalocyanine (MgPc), obtained by probing buffer-gas-cooled molecules with a narrow-linewidth laser. The observed spectrum exhibits a characteristic three-peak pattern, which is well reproduced by modeling MgPc as an oblate symmetric top with D_{4h} symmetry. A key result of this work is that the spectrum is strongly influenced by electronic Coriolis coupling, which is associated with the electronic angular momentum. The electronic Coriolis constant is determined to be approximately 2, indicating an effective orbital angular momentum of about 2 in the excited S_1 state, originating from the π-conjugated ring excitation. This provides a direct spectroscopic signature of electronic angular momentum in a large polyatomic molecule. The presence of nonzero electronic orbital angular momentum is qualitatively consistent with the perimeter model of phthalocyanines. The value lies within the range inferred from previous magnetic circular dichroism (MCD) studies. Compared with the previous MCD estimate, the present analysis provides a more state-specific and narrower constraint, demonstrating that high-resolution spectroscopy enables direct access to electronic and magnetic properties beyond conventional structural characterization.

INTRODUCTION

Phthalocyanines (Fig. 1) are functional dye molecules widely appreciated for their high chemical stability and strong optical transitions in the visible region. They have been extensively explored for applications in optoelectronics and biomedical fields. In addition, owing to their structural similarity to biologically important porphyrins, they serve as prototypical model systems in biomolecular science. Phthalocyanines can coordinate a variety of metal ions at their center, leading to diverse physical and chemical properties depending on the incorporated metal. [1,2]

In particular, their magnetic and magneto-optical properties have attracted considerable interest [1, 2]. The incorporation of different central metal ions gives rise to a wide range of electronic spin configurations, magnetic anisotropies, and spin–orbit coupling effects [3]. For instance, transition-metal phthalocyanines such as copper and cobalt phthalocyanines exhibit paramagnetic behavior due to unpaired d-electrons [3]. Notably, even diamagnetic species such as magnesium and zinc phthalocyanines (MgPc and ZnPc) exhibit pronounced magneto-optical responses originating from orbital contributions of the π-electron system [4, 5]. This indicates that the magnetic properties of phthalocyanines are governed not only by spin states but also by the electronic orbital structure. These features make phthalocyanines valuable model systems for investigating the interplay between electronic structure and magnetism in molecular systems.

Such magneto-optical properties have been extensively studied using techniques such as magnetic circular dichroism (MCD) [1-6], which is highly sensitive to electronic state degeneracies, spin configurations, and Zeeman interactions. MCD measurements have provided important insights into the electronic structure of phthalocyanines, including the nature of their excited states and the influence of the central metal ion. However, their interpretation is often hindered by spectral congestion and limited resolution, particularly for large polyatomic molecules. High-resolution spectroscopy is therefore expected to enable more precise and unambiguous characterization of these magnetically sensitive electronic states.

Although spectroscopic studies of phthalocyanines have been extensive owing to their importance in various contexts [7-15], high-resolution spectroscopy has only recently been explored. Since 2022, partially resolved rotational structures of free-base phthalocyanine (FBPc) and several metal phthalocyanines (MgPc, ZnPc, and chloroaluminum phthalocyanine) have been reported using supersonic expansion [16] and buffer-gas cooling [17-19] techniques. These studies have provided improved rotational constants and, therefore, deeper insights into molecular structure.

In this study, we present an analysis of a high-resolution spectrum of MgPc, which reproduces well the characteristic three-peak pattern observed in the spectrum. The analysis reveals that the Coriolis coupling constant of MgPc is close to 2, indicating an effective orbital angular momentum of approximately 2 associated with the excited state. The presence of nonzero electronic orbital angular momentum can be qualitatively understood within the conventional perimeter model

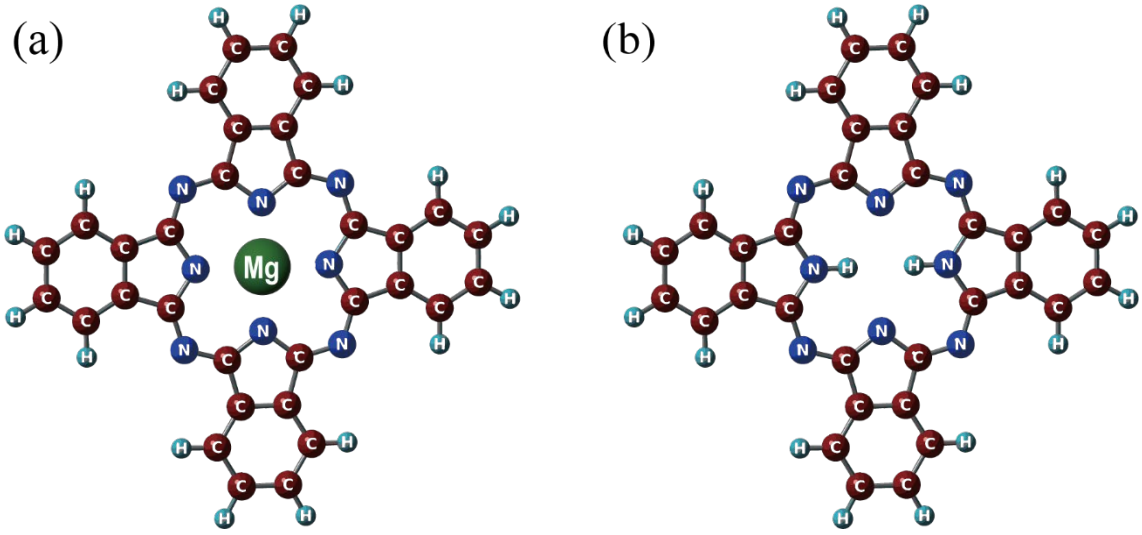

Figure 1: Schematic structures of (a) magnesium-phthalocyanine (MgPc), and (b) free-base phthalocyanine (FBPc).

of phthalocyanines [1,2]. The value of approximately 2 lies within the range inferred from previous MCD results [5]. In contrast to the previous MCD analysis, the present high-resolution analysis provides a more state-specific and narrower constraint.

EXPERIMENTAL

The experimental procedure is largely identical to that described in our previous studies [17-19]. Commercial MgPc (Sigma-Aldrich 402737) was used without further purification. The powder sample, compressed into a solid pellet at 70 MPa, was placed in a buffer-gas cell cooled to approximately 5 K using a pulse-tube cryocooler. Gas-phase MgPc molecules were produced by laser ablation inside the cell using a pulsed Nd:YAG laser (532 nm, ~10 ns pulse width) and subsequently cooled via collisions with helium buffer-gas atoms.

A single-mode ring dye laser (Coherent 699-21, DCM dye) with a power of approximately 10-100 μW was used to record the absorption spectra. The transmitted laser power was detected with a silicon photodiode. The geometrical path length of the probe beam inside the cell was 50 mm. To correct laser intensity fluctuations, a small fraction of the incident beam was sampled prior to entering the cell and used to normalize the incident power of radiation. In addition, the absorbance at a fixed wavelength was continuously monitored using another ring dye laser (Coherent 899, Coumarin 620 dye) with a power of approximately 10-100 μW to track the amount of vaporized MgPc by the ablation laser. This monitoring signal was used for further normalization of the spectra. The laser wavenumber was measured using a wavemeter (HighFinesse WS-6) and calibrated against a Doppler-free saturation spectrum of iodine. The estimated uncertainty was approximately 0.0003 cm^{-1}.

Figure 2 shows the absorption spectrum of buffer-gas-cooled MgPc (red line). The spectrum

clearly exhibits an oscillatory pattern with a period of 0.003 cm^{-1}. This period is almost the same as that of the partially resolved rotational structure of FBPc [17, 18]. Therefore, this pattern can be reasonably assigned to the rotational structure of MgPc. The similarity in the rotational period is expected because the structures of FBPc and MgPc are considered to be similar due to the rigidity of the phthalocyanine ring system. More interestingly, however, there is a distinct difference between their spectra. The oscillatory pattern of MgPc shows a characteristic three-peak structure, whereas that of FBPc exhibits a more uniform oscillation. This marked contrast should be reproduced in the present analysis in order to understand the properties of MgPc.

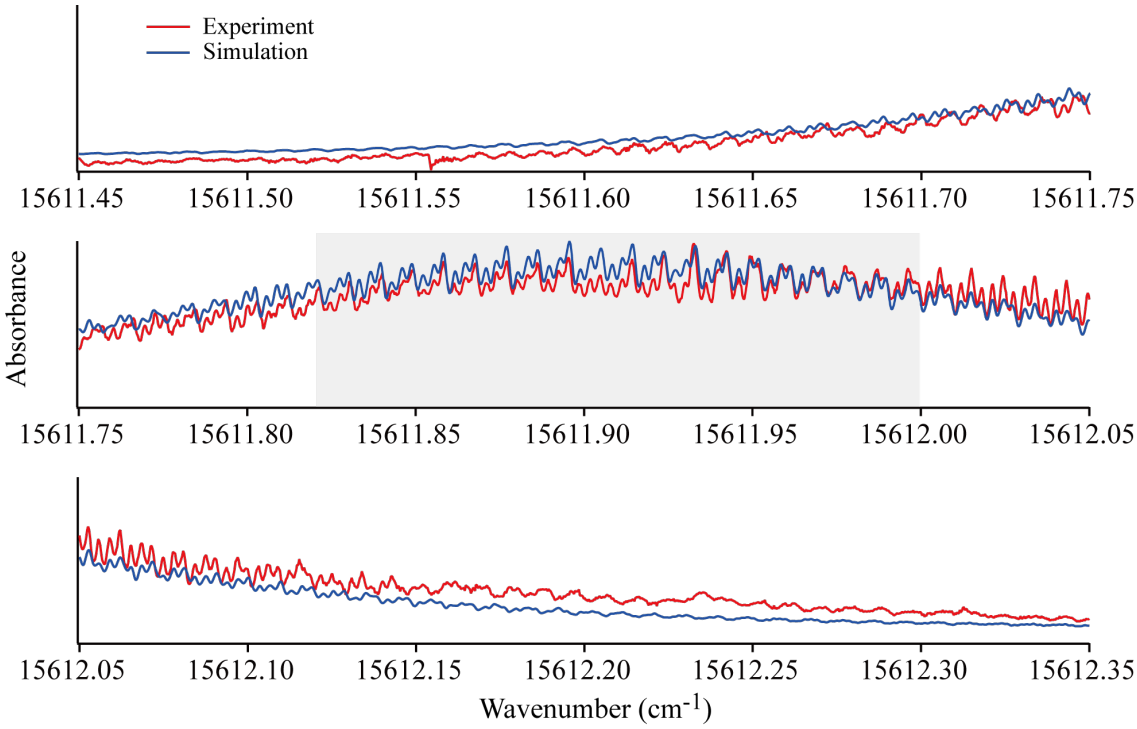

Figure 2: Observed (red) and simulated (blue) spectra of the $S_1 \leftarrow S_0$ transition of MgPc. The gray region indicates the spectral range used for contour fitting.

RESULTS AND DISCUSSION

The structure of MgPc is shown in Fig. 1(a). In the present analysis, MgPc is assumed to be a planar oblate symmetric top with D_{4h} symmetry in both the ground (S_0) and excited (S_1) electronic states. This is in clear contrast to free-base phthalocyanine (FBPc), which is an oblate asymmetric top with D_{2h} symmetry (Fig. 1 (b)), because replacing the central metal ion with two protons lowers the rotational symmetry from fourfold to twofold. We also assume that the S_0 state has A_{1g} symmetry and that the S_1 state is of E_u symmetry. This is another important difference from FBPc, for which the S_1 state has non-degenerate B_{3u} symmetry.

The rotational energy of an oblate symmetric top is given by

$$E_{JK} = BJ(J+1) + (C-B)K^2,$$

where B and C are the rotational constants, J is the rotational quantum number, and K is the projection of the angular momentum onto the molecular axis, which is perpendicular to the molecular plane in MgPc. In previous analyses of FBPc [18], centrifugal distortion terms were included; however, they are neglected in the present study to reduce the complexity of the model.

We find that the Coriolis constant ζ plays a crucial role in reproducing the observed spectrum. This behavior differs from that of FBPc, where the S_1 state is non-degenerate, whereas in MgPc the S_1 state is degenerate due to its higher symmetry. Vibrational Coriolis interactions are known to arise in degenerate vibrational states, where a vibrational angular momentum ζ_v exists (angular momenta are expressed in units of $\hbar$). This interaction couples K and ζ_v, resulting in shifts of the energy levels. Similarly, degenerate electronic states can possess an electronic angular momentum ζ_e, which couples to K via the Coriolis interaction. Since the observed transition corresponds to the 0–0 band, the contribution from the vibrational angular momentum is absent. The rotational energy is therefore modified, to the first order in the Coriolis interaction [20], as

$$E_{JK} = BJ(J+1) + (C-B)K^2 \pm 2\zeta_e CK.$$

In the present E – A transition case, the positive sign is used for $\Delta K = K' - K'' = -1$ transitions, and the negative sign for $\Delta K = +1$ transitions.

Another noteworthy aspect is the nuclear spin statistics, which has rarely been discussed in detail for such large molecules. We evaluated the statistical weights of states, obtaining a ratio of $A_1 : A_2 : B_1 : B_2 : E = 151 : 147 : 151 : 147 : 299$ (indices of gerade/ungerade symmetry are omitted, as they do not affect the relative weights). A summary of this calculation is provided in Appendix A. Although these weights are close to those expected from symmetry-based degeneracy alone, the use of these precise values slightly affects the fitted parameters.

The spectral analysis was carried out using PGOPHER [21]. Initial parameter values were estimated by manually adjusting the rotational constants from those of FBPc, followed by refinement using the contour-fitting function in PGOPHER to reproduce the observed spectral shape. Because the present analysis focuses primarily on the spectral structure near the band center, contour fitting was performed over the spectral range from 15611.82 to 15612.00 cm^{-1}, as indicated by the gray region in Fig. 2. To avoid divergence in the fitting procedure, the parameters of the S_0 and S_1 states were optimized separately in a sequential and iterative manner. Based on the previous analysis of FBPc, the rotational temperature was fixed at 6 K and the translational temperature at 10 K, corresponding to a Doppler width of 0.0016 cm^{-1}. In this analysis, the natural linewidth was neglected because no reliable data are available for the lifetime of the S_1 state in the gas phase, to the best of our knowledge. The S_1 lifetime of FBPc has been reported to be approximately 10 ns [16], corresponding to a linewidth of 0.0005 cm^{-1}. The effects of the above assumptions on the fitted parameters are discussed later.

Figure 2 shows the observed and simulated spectra. The agreement between the experiment

and simulation is reasonably good, particularly in the central region. Even outside the fitting range, the agreement remains satisfactory, supporting the reliability of the fitting. Slight deviations in the oscillatory structure are observed in the outer regions, which may be attributed to the omission of centrifugal distortion terms that become more significant at higher rotational energies. Despite these limitations, the central region of the spectrum is well reproduced, and in particular, the characteristic three-peak pattern is accurately captured. The overall spectral envelope also shows some deviation, which may be due to experimental imperfections such as baseline instability and fluctuations in the ablation process.

In Fig. 3(a), the simulated spectrum (ζ_e = 2.004) is compared with the corresponding stick spectrum, i.e., a spectrum with zero linewidth. For reference, the spectrum calculated with ζ_e = 0 is also shown in Fig. 3(b). The spectrum with $\zeta_e \approx 2$ exhibits a more complex structure with broader branches compared to the ζ_e = 0 case, where groups of lines are more clearly resolved. As discussed in our previous work [17], the oscillatory structures can be understood by assuming that the rotational constants (B and C) are identical for the S_0 and S_1 states, and that $C = B/2$. Under this assumption, the transition energy of the ^rR branch ($\Delta K = +1$, $\Delta J = +1$) can be written as

$$\nu(^rR) = \nu_0 + B(J+1)(J+2) - \frac{B}{2}(K+1)^2 - B\zeta_e(K+1) - BJ(J+1) + \frac{B}{2}K^2$$

$$= \nu_0 + 2B(J+1) - \frac{B}{2}(2K+1) - B\zeta_e(K+1)$$

$$= B[2J - (1+\zeta_e)K] + \nu_0 + \left(\frac{3}{2} - \zeta_e\right)B,$$

where ν_0 is the band origin. Similarly, the transition energy of the ^pP ($\Delta K = -1$, $\Delta J = -1$) branch is given by

$$\nu(^pP) = \nu_0 + BJ(J-1) - \frac{B}{2}(K-1)^2 + B\zeta_e(K-1) - BJ(J+1) + \frac{B}{2}K^2$$

$$= \nu_0 - 2BJ + \frac{B}{2}(2K-1) + B\zeta_e(K-1)$$

$$= B[-2J + (1+\zeta_e)K] + \nu_0 - \left(\frac{1}{2} + \zeta_e\right)B.$$

Note that the ^rR and ^pP branches are generally more intense than the other branches. When ζ_e = 0, transitions with constant $2J - K$ form groups of lines separated by approximately B, since $2J - K$ takes integer values. As shown in Fig. 3(b), transitions such as $^pP_{25}(25)$, $^pP_{23}(24)$, $^pP_{21}(23)$, $^pP_{19}(22)$, … with $2J - K = 25$ form such a cluster. This behavior is consistent with that observed for FBPc in our previous study. Here, the notation $^{\Delta K}\Delta J_{K''}(J'')$ is used. When $\zeta_e \approx 2$, transitions with constant $2J - 3K$ form similar clusters. As shown in Fig. 3(a), transitions such as $^rR_{25}(25)$, $^rR_{27}(28)$, $^rR_{29}(31)$, $^rR_{31}(34)$, … with $2J - 3K = -25$ cluster together. Since $2J - 3K$ also takes integer values, the spacing between these

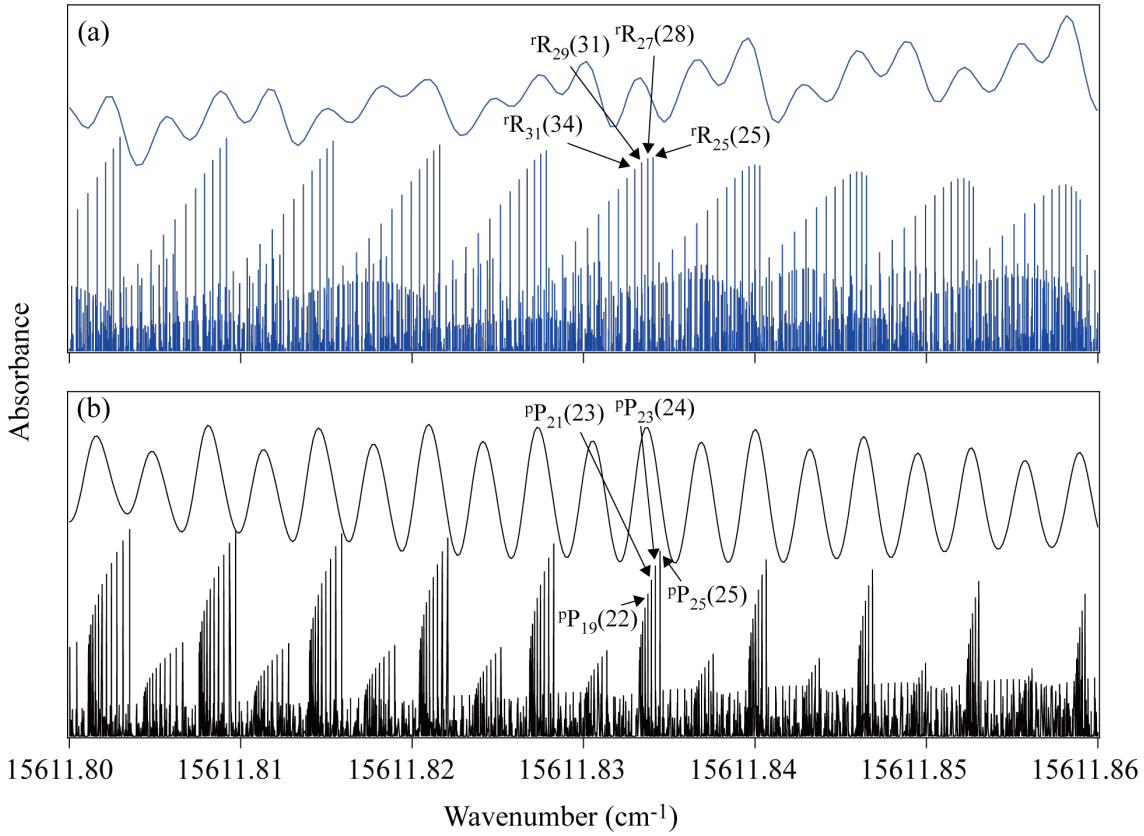

Figure 3: Simulated and stick spectra: (a) with a Coriolis constant of 2.004 and (b) without Coriolis coupling. Assignments of selected transitions are indicated. Note that the intensities of degenerate lines are not summed in the stick spectra.

groups is close to the value of *B*, although the grouping becomes less distinct due to the increased spectral complexity. The intense series originate from the E symmetry nuclear-spin states in the S_1 state, while weaker series arise from the A and B symmetry states. This intensity modulation is clearly seen in Fig. 3(a). Nevertheless, the combined intensity of the A and B symmetry states remains comparable to that of the E state because the A and B states are degenerate. According to the above discussion, the overall oscillatory patterns of MgPc and FBPc are similar, although their detailed structures differ. While this simplified model does not fully reproduce the observed three-peak structure, it provides useful insight into the underlying spectral features.

The fitted parameters are listed in Table 1 together with those of FBPc reported previously [18]. The fitting uncertainties are given in parentheses and are approximately one order of magnitude smaller than those obtained for FBPc. This reduction may be attributed to the smaller number of fitted parameters and the restricted fitting range. It should be noted, however, that these uncertainties reflect only the fitting errors and do not account for experimental uncertainties; therefore, the true uncertainties are expected to be larger. Figure 4 compares the observed spectrum with spectra calculated using ζ_e = 2.004, 1.954, and 2.054, while keeping all other parameters fixed at the values

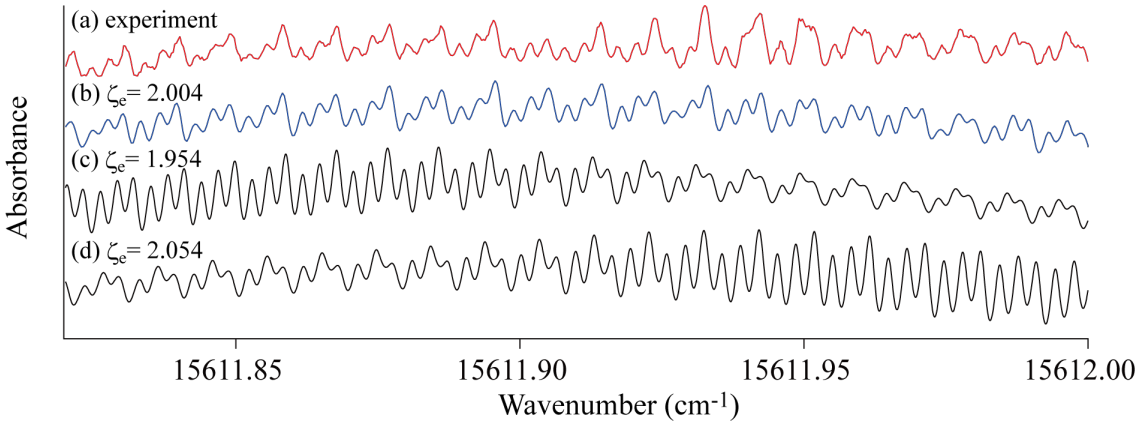

Figure 4 : Comparison of the observed spectrum (a) with spectra calculated using ζ_e = 2.004 (b), 1.954 (c), and 2.054 (d).

listed in Table 1. The oscillatory patterns obtained with ζ_e = 1.954 and 2.054 clearly deviate from the observed spectrum. Although it remains possible that the observed pattern could be reproduced by adjusting other rotational constants together with these ζ_e values, the present fit is clearly sensitive to ζ_e. On this basis, the effective uncertainty in ζ_e around the present local minimum of the fitting residual is estimated to be less than 0.05. Similarly, sensitivity tests indicate that variations of approximately 1×10^{-5} cm^{-1} in the rotational constants lead to noticeable changes in the spectral shape. We also performed sensitivity tests by varying the rotational temperature from 4 to 8 K, the translational temperature from 6 to 15 K, the Lorentzian linewidth from zero to 0.0005 cm^{-1}, and the fitting interval from the original range of 15611.82-15612.00 cm^{-1} to as wide as 15611.62-15612.20 cm^{-1}. Each of these conditions was varied individually, and the fitting procedure was repeated for each case. We also examined the influence of centrifugal-distortion terms by repeating the fitting with the constants fixed at the values reported for FBPc [18]. The fitted rotational constants changed by at most 2.3×10^{-6} cm^{-1}, the band origin changed by at most 1×10^{-4} cm^{-1}, and ζ_e changed by at most 0.005. These variations are larger than the fitting errors obtained from PGOPHER. Because the present tests do not constitute a complete statistical uncertainty analysis, we conservatively assign practical uncertainties of 1×10^{-5} cm^{-1} to the rotational constants, 5×10^{-4} cm^{-1} to the band origin, and 0.05 to ζ_e.

All rotational constants of MgPc are approximately 4% larger than those of FBPc, indicating that MgPc has a slightly more compact structure. The inertial defects of the S_0 and S_1 states are 7.0 and −14 u Å^2, respectively, which are somewhat larger than those of FBPc. However, considering the uncertainty at the 10^{-5} level in the rotational constants, these values are effectively consistent with zero, supporting a planar molecular structure within the present accuracy.

The Coriolis constant ζ_e is

$$\zeta_e = \int \psi_e^* L_z \psi_e d\tau_e,$$

where ψ_e is the electronic wavefunction and L_z is the z-component of the electronic angular momentum, with the z-axis along the C_4 symmetry axis. This expression indicates that ζ_e represents the projection of the electronic orbital angular momentum. The z-component of the electronic angular momentum is generally not a good quantum number and may take non-integer values.

In phthalocyanines, the non-zero orbital angular momentum can be interpreted within the framework of the traditional perimeter model, which has been widely used to explain the strong Soret bands and weak Q bands in phthalocyanines and porphyrins [1, 2]. In this model, 18 electrons occupy the π-conjugated orbitals of the 16-membered ring. Two additional electrons can be effectively attributed to the central metal. The central metal can be treated as Mg^{2+}, indicating that it has no valence electrons and is diamagnetic. The π system consists of 16 orbitals with angular momentum quantum numbers $k = 0, \pm 1, \ldots, \pm 7, 8$ along the molecular axis. In the ground state, the total angular momentum is zero, while excited states can carry finite angular momentum. Since the HOMO corresponds to $k = \pm 4$ and the LUMO to $k = \pm 5$, the lowest excited states may have angular momentum of 1 or 9, corresponding to transitions with $\Delta k = 1$ or 9. The former gives rise to the intense Soret band, while the latter corresponds to the weaker Q band. Although this model is qualitative, it successfully captures the essential features of the electronic transitions and suggests a non-zero orbital angular momentum for the S_1 state.

Recently, MCD studies of MgPc have been reported [5]. MCD probes the magnetic response of electronic transitions using circularly polarized light and is closely related to Zeeman spectroscopy, providing direct access to magnetic dipole properties. Although the analysis of MCD spectra is often complicated by spectral congestion, previous studies have reported that the S_1 state of MgPc has $|L_z| \approx 1$–3 [5]. Furthermore, a theoretical calculation predicted an angular momentum of 3.13 for the S_1 state of phthalocyanines [4]. These values are consistent in magnitude with the present result. The present high-resolution spectroscopic analysis is based on the rotational structure of a specific rovibronic band and provides a more state-specific and narrower constraint. These results highlight the advantage of high-resolution spectroscopy in investigating the electronic structure and magneto-optical properties of large molecules.

Table 1: Summary of spectroscopic constants of the S_0 and S_1 states of MgPc and FBPc. *A*, *B*, and *C* are rigid-rotor rotational constants. T_0 is a band origin. Single (double) primes denote constants for the S_1 (S_0) state. ζ_e is the Coriolis constant of the S_1 state. All values are given in cm^{-1}, except for ζ_e. Numbers in parentheses represent fitting errors obtained from PGOPHER and indicate the precision of the fit; the practical uncertainties are discussed in the text.

	MgPc (This study)	FBPc [18]
A'' (x10^{-3})		2.9899(40)
B'' (x10^{-3})	3.1112(3)	2.9760(13)
C'' (x10^{-3})	1.5546(1)	1.4916(24)
T_0	15611.91365(5)	15131.6882
A' (x10^{-3})		2.9804(31)
B' (x10^{-3})	3.1061(2)	2.9783(22)
C' (x10^{-3})	1.5550(1)	1.4901(24)
ζ_e	2.004(1)	

SUMMARY

The high-resolution S_1–S_0 spectrum of MgPc was analyzed and successfully reproduced by assuming an oblate symmetric-top structure with D_{4h} symmetry. The spectral structure is markedly different from that of FBPc reported previously, demonstrating the enhanced level of detail accessible through high-resolution spectroscopy.

A key finding of this study is that Coriolis coupling associated with electronic angular momentum plays a crucial role in reproducing the observed spectrum. The Coriolis constant is determined to be approximately 2, indicating an effective orbital angular momentum of about 2 in the excited S_1 state, originating from the π-conjugated ring system. This result provides a direct spectroscopic signature of electronic angular momentum in a large polyatomic molecule.

The presence of nonzero electronic orbital angular momentum is qualitatively consistent with the perimeter model of phthalocyanines. The value of approximately 2 lies within the range inferred from previous MCD studies. The present high-resolution spectroscopic analysis is based on the rotational structure of a specific rovibronic band and provides a more state-specific and narrower constraint.

These results demonstrate that high-resolution spectroscopy can provide not only structural information but also direct insight into electronic and magneto-optical properties, opening a new avenue for probing the electronic and magnetic properties of complex molecular systems. Future work will involve combining high-resolution spectroscopy with external electric and magnetic fields. Such approaches are expected to enable more direct and precise determination of molecular properties, including dipole moments, magnetic responses, and electronic angular momenta, thereby providing deeper insight into the electronic structure and dynamics of complex molecular systems. It is also worth noting that ab initio calculations for MgPc would provide valuable insight not only into its molecular structure but also into its electronic properties.

APPENDIX A. Nuclear Spin Statistical Weights of MgPc

In this Appendix, we outline the estimation of the nuclear spin statistical weights used in the present analysis and clarify how the approximate expression employed in the main text is obtained. Because

the gerade/ungerade distinction is not important for the present discussion, these indices are omitted unless otherwise noted.

First, the nuclear spin functions must be classified into irreducible representations of the molecular symmetry group. Magnesium phthalocyanine (MgPc) belongs to the D_{4h} point group. Since there is only one Mg nucleus located at the center, it does not contribute to permutation symmetry and can be excluded from the nuclear spin analysis. The phthalocyanine ring system ($C_{32}H_{16}N_8$) can be regarded as consisting of four equivalent structural units,

$$^{12}C_8{}^{1}H_4{}^{14}N_2.$$

As shown below, the nuclear spin states can be classified by considering symmetry operations acting on these four units. The nuclear spins of the constituent atoms are

$$^{12}C: I_C = 0$$

$$^{1}H: I_H = 1/2$$

$$^{14}N: I_N = 1$$

Thus, the number of nuclear spin functions for one unit is

$$(2I_C + 1)^8 \times (2I_H + 1)^4 \times (2I_N + 1)^2$$

$$= 1^8 \times 2^4 \times 3^2 = 16 \times 9 = 144.$$

Because the molecule consists of four equivalent units, the total number of nuclear spin functions is

$$N_{ns} = 144^4 = 429{,}981{,}696.$$

This number represents all possible nuclear spin configurations without considering symmetry.

The symmetry operations relevant to MgPc correspond to permutations of the four equivalent units combined with inversion. Therefore, the nuclear spin functions form a representation of the permutation-inversion group acting on these units, which is called the molecular symmetry group. For MgPc, the molecular symmetry group $D_{4h}(M)$ is used [22], which is isomorphic to the point group D_{4h}.

The multiplicities of the irreducible representations were evaluated by counting the number of nuclear spin configurations that remain invariant under each symmetry operation [23]. Here, the four equivalent units are labeled 1–4. For each operation E, (1234), (13)(24), (13), and (12)(34), the number of invariant configurations was determined. For example, under the operation (13)(24), the units 1 and 3 must have identical spin configurations, and the units 2 and 4 must also be identical, while the two pairs can differ from each other. Therefore, the number of invariant configurations is 144^2. Similarly, for the operation (13), the units 1 and 3 must be identical, while the remaining units are independent, giving 144^3. The number of invariant configurations obtained for each symmetry operation corresponds to the character of the nuclear spin representation. Using these characters and the character table of the symmetry group, the representation can be decomposed into irreducible components, yielding

$$54{,}502{,}020\ A_1 \oplus 52{,}998{,}660\ A_2 \oplus 54{,}491{,}580\ B_1 \oplus 53{,}008{,}956\ B_2 \oplus 107{,}490{,}240\ E.$$

The above decomposition indicates how the enormous number of nuclear spin functions is distributed among symmetry species. For spectroscopic applications, only relative weights are important, and the overall scale is irrelevant. To obtain a compact and practical expression, the above coefficients can be divided by a common factor. First, dividing by $2^2 3^2$ gives

$$1{,}513{,}945\ A_1 \oplus 1{,}472{,}185\ A_2 \oplus 1{,}513{,}655\ B_1 \oplus 1{,}472{,}471\ B_2 \oplus 2{,}985{,}840\ E.$$

These values are still too large for practical use in the PGOPHER analysis, so they were further reduced to

$$151\ A_1 \oplus 147\ A_2 \oplus 151\ B_1 \oplus 147\ B_2 \oplus 299\ E.$$

Our analysis used these values. If the original coefficients are normalized by the A_1 value, the relative ratios become

$$1\ A_1 \oplus 0.9724\ A_2 \oplus 0.9998\ B_1 \oplus 0.9726\ B_2 \oplus 1.9722\ E.$$

Thus, the E representation has a weight approximately twice as large as those of the other symmetry species. This is quite reasonable because the multiplicity a_μ of an irreducible representation μ is given by

$$a_\mu = \frac{1}{g}\sum_{\hat{R}} \chi^{\mathrm{red}}(\hat{R})\chi^{\mu}(\hat{R})^{*},$$

where g is the order of the group, $\hat{R}$ denotes the symmetry operations in the group, χ^{μ} is the character of the irreducible representation, and χ^{red} is the character of the reducible representation to be decomposed. For large molecules, the character of the identity operation ($\hat{E}$) is usually much larger than those of the other symmetry operations. In the case of MgPc, $\chi^{\mathrm{red}}(\hat{E}) = 144^4$, whereas the other characters are at most on the order of 144^3. Therefore,

$$a_\mu \sim \frac{1}{g}\chi^{\mathrm{red}}(\hat{E})\chi^{\mu}(\hat{E})^{*}.$$

Because the character of the identity operation is equal to the dimension of the irreducible representation, the E representation naturally has nearly twice as many states as each of the one-dimensional representations.

The Pauli principle connects the above nuclear spin states with the states of the other degrees of freedom, i.e., the rovibronic wavefunctions. Because each unit contains an even number of each type of atoms, it can be treated as a boson. Therefore, the total wavefunction must be symmetric under exchange of the units. This requirement is equivalent to the condition that the direct product of the irreducible representations of the nuclear spin and rovibronic wavefunctions must contain the A_1 representation. As a result, a rovibronic state with symmetry Γ is associated with nuclear spin states of the same symmetry Γ. We can therefore estimate the nuclear spin statistical weight of each rovibronic state.

ACKNOWLEDGEMENTS

Y.M. would like to thank the members of Core for Quantum Universe (RIIS, Okayama University). This work was supported by JSPS KAKENHI Grant Nos. JP18H01229, JP22H01249, and JP23K03277.

AUTHOR DECLARATIONS

Conflict of Interest

The authors have no conflicts to disclose.

Author Contributions

Y. Miyamoto: Conceptualization (equal); Data Curation (lead); Funding Acquisition (lead); Investigation (lead); Methodology (equal); Project Administration (lead); Validation (lead); Visualization (lead); Writing – original draft (lead). **K. Enomoto**: Conceptualization (equal); Funding Acquisition (supporting); Methodology (equal); Writing – review and editing (equal). **K. Iwakuni:** Conceptualization (equal); Funding Acquisition (supporting); Methodology (equal); Writing – review and editing (equal). **S. Kuma**: Conceptualization (equal); Funding Acquisition (supporting); Methodology (equal); Writing – review and editing (equal). **K. M. T. Yamada**: Formal Analysis (equal); Writing – review and editing (equal).

DATA AVAILABILITY

The data that support the findings of this study can be obtained from the corresponding author upon reasonable request.

REFERENCES

[1] H. Isago, Optical Spectra of Phthalocyanines and Related Compounds (Springer, Tokyo, 2015), doi:10.1007/978-4-431-55102-7.

[2] T. Fukuda and N. Kobayashi, Electronic Absorption Spectra—Phthalocyanines, in Handbook of Porphyrin Science, Vol. 9, ed. by K. M. Kadish, K. M. Smith, and R. Guilard (World Scientific, 2010), doi:10.1142/7752-vol9.

[3] J. Bartolomé, C. Monton, and I. K. Schuller, “Magnetism of Metal Phthalocyanines,” in Molecular Magnets, ed. by J. Bartolomé, F. Luis, and J. Fernández (Springer, Berlin, Heidelberg, 2014), doi:10.1007/978-3-642-40609-6_9.

[4] A. J. McHugh, M. Gouterman, and C. Weiss, “Porphyrins XXIV. Energy, oscillator strength, and Zeeman splitting calculations (SCMO-CI) for phthalocyanine, porphyrins, and related ring systems,” Theor. Chim. Acta 24, 346–370 (1972), doi:10.1007/BF01007552.

[5] S. Suzuki, A. Santria, T. Oyama, K. Akao, and N. Ishikawa, “Electronic structure analysis of

phthalocyanine complexes using magnetic circular dichroism and magnetic circularly polarized luminescence spectroscopy," Chirality 2024, e23625, doi:10.1002/chir.23625.
[6] N. Kobayashi and K. Nakai, "Applications of magnetic circular dichroism spectroscopy to porphyrins and phthalocyanines," Chem. Commun. 2007, 4077–4092, doi:10.1039/B704991A.
[7] L. Edwards and M. Gouterman, "Porphyrins XV. Vapor absorption spectra and stability: Phthalocyanines," J. Mol. Spectrosc. 33, 292–310 (1970), doi:10.1016/0022-2852(70)90040-8.
[8] V. E. Bondybey and J. H. English, "Spectra of the H_2 phthalocyanine in low-temperature matrices," J. Am. Chem. Soc. 101, 3446–3450 (1979), doi:10.1021/ja00507a004.
[9] P. S. H. Fitch, L. Wharton, and D. H. Levy, "The fluorescence spectrum of free base phthalocyanine cooled in a supersonic free jet," J. Chem. Phys. 70, 2018–2028 (1979), doi:10.1063/1.437629.
[10] P. S. H. Fitch, C. A. Haynam, and D. H. Levy, "The fluorescence excitation spectrum of free base phthalocyanine cooled in a supersonic free jet," J. Chem. Phys. 73, 1064–1072 (1980), doi:10.1063/1.440278.
[11] J. A. Menapace and E. R. Bernstein, "Spectroscopic studies of phthalocyanines and their clusters with small molecules," J. Chem. Phys. 87, 6877–6886 (1987), doi:10.1063/1.453382.
[12] F. L. Plows and A. C. Jones, "Laser-desorption supersonic jet spectroscopy of phthalocyanines," J. Mol. Spectrosc. 194, 163–170 (1999), doi:10.1006/jmsp.1998.7796.
[13] M. Hartmann, A. Lindinger, J. P. Toennies, and A. F. Vilesov, "The phonon wings in the S_1–S_0 spectra of tetracene, pentacene, porphin and phthalocyanine in liquid helium droplets," Phys. Chem. Chem. Phys. 4, 4839–4844 (2002), doi:10.1039/B203249J.
[14] R. Lehnig, M. Slipchenko, S. Kuma, T. Momose, B. Sartakov, and A. Vilesov, "Fine structure of the S_1–S_0 band origins of phthalocyanine molecules in helium droplets," J. Chem. Phys. 121, 9396–9405 (2004), doi:10.1063/1.1804945.
[15] A. Slenczka, "Electronic spectroscopy of phthalocyanine and porphyrin derivatives in superfluid helium nanodroplets," Molecules 22, 1244 (2017), doi:10.3390/molecules22081244
[16] F. Schlaghaufer and A. Slenczka, "Electronic spectroscopy of phthalocyanine in a supersonic jet revisited," Phys. Chem. Chem. Phys. 24, 20921–20926 (2022), doi:10.1039/D2CP02256G.
[17] Y. Miyamoto, R. Tobaru, Y. Takahashi, A. Hiramoto, K. Iwakuni, S. Kuma, K. Enomoto, and M. Baba, "High-resolution spectroscopy of buffer-gas-cooled phthalocyanine," Commun. Chem. 5, 161 (2022), doi:10.1038/s42004-022-00783-4.
[18] Y. Miyamoto, A. Hiramoto, K. Iwakuni, S. Kuma, K. Enomoto, N. Nakayama, and M. Baba, "Analysis on high-resolution spectrum of the S_1–S_0 transition of free-base phthalocyanine," J. Chem. Phys. 160, 144304 (2024), doi:10.1063/5.0191810.
[19] Y. Miyamoto, M. Baba, K. Enomoto, A. Hiramoto, K. Iwakuni, and S. Kuma, "High-resolution electronic spectroscopy of buffer-gas-cooled metal-phthalocyanines," Low Temp. Phys. 50, 808–812

(2024), doi:10.1063/10.0028188.
[20] G. Herzberg, Molecular Spectra and Molecular Structure. Vol. III: Electronic Spectra and Electronic Structure of Polyatomic Molecules (D. Van Nostrand, Princeton, 1967).
[21] C. M. Western, “PGOPHER: A program for simulating rotational, vibrational and electronic spectra,” J. Quant. Spectrosc. Radiat. Transfer 186, 221–242 (2017), doi:10.1016/j.jqsrt.2016.04.010.
[22] P. R. Bunker and P. Jensen, Molecular Symmetry and Spectroscopy, 2nd ed. (NRC Research Press, Ottawa, 1998).
[23] L. D. Landau and E. M. Lifshitz, Quantum Mechanics, 2nd ed., translated by J. B. Sykes and J. S. Bell (Pergamon Press, London, 1958).